DOI: 10.26599/FSHW.2025.9250887

Contents lists available at SciOpen

Food Science and Human Wellness

journal homepage: https://www.sciopen.com/journal/2097-0765

China Food Publishing Co.

A flexible and reusable self-assembled SERS sensor: One-step sampling and on-site detection of bifenthrin in foods

Yingfang Zhang[1], Guanyong Liu[2], Chen Chen[1], Geoffrey I.N. Waterhouse[3], Xuguang Qiao[1], Zhixiang Xu[1*]

[1]*Key Laboratory of Food Processing Technology and Quality Control in Shandong Province, College of Food Science and Engineering, Shandong Agricultural University, Tai'an 271018, People's Republic of China*

[2]*BinZhou Polytechnic, Binzhou 256603, People's Republic of China*

[3]*School of Chemical Sciences, The University of Auckland, Auckland 1142, New Zealand*

ABSTRACT: A reusable and flexible surface-enhanced Raman spectroscopy (SERS) sensor was constructed through an interfacial assembling strategy for rapid and non-destructive detection of bifenthrin in foods. The sensor was fabricated through rational integration of two components: (1) a plasmonic ternary Au@Cu_2O@Ag nanoarrays synthesized via liquid-liquid interface self-assembly (LLISA) on Teflon tape, and (2) an epoxy resin (EP) encapsulation layer. The Au@Cu_2O@Ag nanoarrays demonstrated exceptional SERS performance due to synergistic plasmonic enhancement effects from the Au core, charge transfer mediation via the Cu_2O interlayer, and secondary electromagnetic field amplification by the Ag shell. The Teflon tape ensured uniformity of the SERS "hot spots", while EP encapsulation provided mechanical durability and oxidation resistance. Unlike traditional methods (e.g., HPLC, GC) requiring extensive pretreatment and hours-long analysis, the flexible SERS sensor allowed one-step and pretreatment-free sampling and on-site detection of bifenthrin on irregular food surfaces, delivering laboratory-grade quantification of bifenthrin within 3 minutes. Under optimal testing conditions, the sensor exhibited a low limit of detection (1.81×10^{-9} μmol/L) and a wide linear response range of 10^{-8}-10^{3} μmol/L. Additionally, the flexible SERS sensor demonstrated high accuracy in bifenthrin-spiked food samples with recoveries of 94.18%-104.53%. Notably, the developed sensor exhibited practical applicability in bifenthrin quantification across four real food samples, demonstrating excellent agreement with standard gas chromatography (GC), thereby validating the reliability of the proposed method.

Keywords: Surface-enhanced Raman spectroscopy; Flexible SERS sensor; Liquid-liquid interface self-assembly; Bifenthrin detection

1. Introduction

Bifenthrin, a third-generation synthetic pyrethroid, has emerged as a cornerstone insecticide in global agrochemical practices due to its exceptional photostability, broad-spectrum efficacy, and prolonged residual activity[1]. Despite the agricultural merits of bifenthrin, its bioaccumulative nature and lipophilicity can lead to persistent residues in food matrices, posing neurotoxic risks to humans through chronic exposure[2-3].

***Corresponding author**
zhixiangxu@sina.com (Zhixiang Xu)

Received 28 July 2025
Received in revised from 15 August 2025
Accepted 10 September 2025

Furthermore, various studies have reported that bifenthrin residues are common in most agricultural commodities, which has caused significant public concern[4-5]. The development of an accurate, sensitive, and rapid detection method for bifenthrin residues is critical to ensuring food safety and mitigating neurotoxic risks associated with chronic human exposure.

To date, numerous chromatographic techniques have been reported for bifenthrin quantification, including high-performance liquid chromatography (HPLC) and gas chromatography-mass spectrometry (GC-MS)[6-8]. However, these methods require labor-intensive procedures, time-consuming column purification, and expert personnel. Consequently, these methods are impractical for high-throughput or on-site applications. To overcome these limitations, rapid sensing platforms such as immunoassays, electrochemical sensors, and surface-enhanced Raman spectroscopy (SERS) have emerged as promising alternatives[9-11]. SERS due to its fingerprint specificity, single-molecule sensitivity, and on-site deployment capabilities is very promising for food safety surveillance[12-13].

Surface-enhanced Raman spectroscopy (SERS) relies on plasmonic nanostructures to amplify analyte signals through local surface plasmon resonances (LSPRs) and chemical enhancement mechanisms[14-15]. Ag nanoparticles (Ag NPs) exhibit unparalleled electromagnetic enhancement due to intense LSPRs at visible wavelengths. However, the rapid surface oxidation of silver nanoparticles (Ag NPs) under ambient conditions compromises SERS substrate stability. Au nanoparticles (Au NPs) offer superior chemical stability but at the expense of lower LSPR intensity. Cu-based materials, though cost-effective, exhibit weak plasmonic activity. To overcome these trade-offs, researchers have been exploring combinations of noble metals with transition metal oxides[16]. Despite advances in plasmonic nanostructure design, achieving precise interparticle gap to generate high-density electromagnetic "hot spots" remains a persistent challenge in SERS substrate fabrication[17]. Recent studies have shifted toward self-assembled nanoarrays, which achieve control over nanoparticle spacing through interfacial phenomena[18]. Among these strategies, liquid-liquid interface self-assembly (LLISA) distinguishes itself by enabling scalable fabrication of monolayer nanoarrays (up to 10 × 10 cm^2) with < 10% interparticle spacing variation, a key feature for achieving spatially uniform signal enhancement in SERS substrates[19-22].

While LLISA enables precise control over plasmonic nanoarray architectures, it has traditionally been implemented on rigid planar substrates (e.g., silicon wafers) often resulting in multilayer stacks of nanoparticles during assembly[23]. This stacking disrupts the uniformity of electromagnetic “hot spots”, leading to inconsistent SERS signals and detection inaccuracies[24-25]. To address this problem, flexible substrates have emerged as an effective strategy to prevent the undesirable stacking of nanoparticles[26-28]. Teflon tape, with inherent hydrophobicity and flexibility, exhibits several advantages for LLISA applications: (1) Interfacial Confinement: The inherent hydrophobicity of Teflon tape localizes nanoparticle assembly exclusively at the oil-water interface during LLISA, thereby preventing aqueous-phase aggregation[29]; (2) Chemical Inertness: Teflon tape confers exceptional resistance to acidic, alkaline, and organic solvent environments, thereby enabling its reliable deployment in chemically heterogeneous food systems[30]. (3)

Mechanical Compliance: With flexibility and a high tensile strength, Teflon tape helps to maintain nanoarray integrity during glove flexion, achieving good signal retention[31]. Therefore, Teflon tape can be combined with gloves to build flexible SERS platforms that integrate sampling and detection into a single step, fulfilling the essential requirements for rapid real-time food safety monitoring. Furthermore, to address critical challenges in nanoparticle adhesion and operational durability, epoxy resins (EP) are also important for sensor design. EPs offer three distinct advantages[32-33]: (1) Mechanical Stress Dissipation: The viscoelastic network of cured EP absorbs and redistributes shear forces during flexible substrate (e.g., glove) deformation, effectively preventing nanoparticle delamination or "hot spots" disruption. (2) Environmental Passivation: The dense crosslinked structure of EP acts as a barrier against oxygen and moisture diffusion, greatly reducing the metal oxidation rates and ensuring long-term mechanical stability. (3) Enhanced Reusability: The chemical inertness and structural integrity of EP ensure sustained SERS intensity retention after several cleaning-reuse cycles, ensuring exceptional recyclability for cost-effective operations.

In the present study, a flexible EP/Au@Cu_2O@Ag/Teflon tape SERS sensor was fabricated through sequential steps (Scheme 1a, b and c): Au@Cu_2O@Ag NPs were first synthesized via a seed-mediated growth strategy, then assembled into ordered nanoarrays at a cyclohexane/water interface using the LLISA method. Subsequently, the nanoarrays were encapsulated with an epoxy resin (EP), and transferred onto gloves via adhesive Teflon tape. The resulting flexible and reusable EP/Au@Cu_2O@Ag/Teflon tape SERS sensor was then successfully applied for on-site detection of bifenthrin in food. The prepared sensor combines a flexible Teflon substrate, uniform monolayer nanoarrays assembly with a high-density of SERS "hot spots", and an EP layer for maintaining mechanical durability and high SERS enhancements under a variety of extreme environmental conditions. Additionally, the flexible SERS sensor enables one-step sampling and on-site analysis within 3 minutes, achieving reliable in-situ detection of bifenthrin on irregular food surfaces without any pretreatment (Scheme 1 d). To our knowledge, this study establishes the first demonstration of EP/Au@Cu_2O@Ag/Teflon tape as a flexible SERS substrate for on-site ultrasensitive and reproducible monitoring of bifenthrin in foods.

Scheme 1. Schematic illustration of (a) Au@Cu_2O@Ag fabrication, (b) the specific process of self-assembly, (c) EP/Au@Cu_2O@Ag/Teflon tape flexible SERS sensor fabrication (d) performance and advantages of the EP/Au@Cu_2O@Ag/Teflon tape flexible SERS sensor.

2. Experimental sections

2.1 Material, chemicals and apparatus

Pepper, eggplant, rape, tomato, cauliflower, cucumber, Chinese cabbage, kiwifruit, grapes, pomelo, strawberry, blueberry, orange, apple, pear, calibrated sprayer and stainless steel tweezers were purchased from a local supermarket in Tai'an (Shandong, China).

Bifenthrin was obtained from Hubei Xinrunde Chemical Co., Ltd. (Wuhan, China). Tetrachloroauric (III) acid tetrahydrate ($HAuCl_4 \cdot 4H_2O$) and trisodium citrate dihydrate ($C_6H_5Na_3O_7 \cdot 2H_2O$) were obtained

from Tianjin Kaitong Chemical Reagent Co., Ltd. (Tianjin, China). Polyvinyl pyrrolidone (PVP K30) was purchased from Sichuan Weikeqi Biological Techn. Co., Ltd. (Chengdu, China). Copper(II) nitrate trihydrate ($Cu(NO_3)_2 \cdot 3H_2O$) and diluted hydrazine hydrate aqueous solution ($N_2H_4 \cdot H_2O$, 85%), silver nitrate ($AgNO_3$), anhydrous ethanol and deionized water were sourced from Tianjin Kemiou Chemistry Reagent Co., Ltd. (Tianjin, China). Cyclohexane, glucose, ascorbic acid, sodium ions, magnesium ions, chloride ions, sulfate ions, L-Histidine, L-Lysine, aniline, phenol, 1-naphthol, benzimidazole were supplied by Beijing Solarbio Science & Technology Co., Ltd. (Beijing, China). Bisphenol A epoxy resin (EP) was obtained from Ricci New Materials Co., Ltd. (Guangzhou, China). Teflon tape was purchased from DETAI TAPE Co., Ltd. (Guangzhou, China). Disposable nitrile gloves were obtained from Jiangsu Yangzilide Medical Equipment Co., Ltd. (Jiangsu, China).

Raman spectra were obtained on a handheld Raman spectrometer (OH-OEM 10-0045). The laser wavelength used was 785 nm, the laser power was 8 W, and the integration time was 2 s. Scanning electron microscopy (SEM) images were acquired using a field emission scanning electron microscope (Sigma 500, ZEISS, Germany). Ultraviolet-visible (UV-vis) spectra were collected at room temperature on a UV-5500 spectrophotometer (Shimadzu Co., Kyoto, Japan). Dynamic light scattering (DLS) analyses of the prepared nanoparticles were performed on a laser nanometer particle size analyzer (Malvern, England).

The GC system used in this work for the determination of bifenthrin was a Hewlett-Packard 6890 (Agilent Technologies, USA) equipped with split injector and an electron capture detector (ECD, ^{63}Ni). An Rtx-1 capillary column (cross bonded 100% dimethyl polysiloxane, 30 m × 0.25 mm) with a film thickness of 0.25 μm (RESTEK, USA) was applied to separate bifenthrin from other compounds. Nitrogen was used as carrier gas (flow rate of 1 mL/min) and makeup gas (30 mL/min). The splitless mode was used for all sample injections (injection volume of 1 μL). The GC column temperature was ramped as follows: the initial temperature was 150 ℃ and maintained for 2 min, then the temperature was gradually raised to 270 ℃ at a rate of 6 ℃/min and maintained at this temperature for 16 min. The temperature of injector and detector were set at 200 ℃ and 320 ℃, respectively.

2.2 Synthesis of Au@Cu_2O@Ag nanoarray with Teflon tape (Au@Cu_2O@Ag/Teflon tape)

100 mL of an aqueous $HAuCl_4 \cdot 4H_2O$ solution (2.4×10^{-4} M) and 4 mL of an aqueous $C_6H_5Na_3O_7 \cdot 2H_2O$ solution (0.034 M) were mixed and heated for 30 min under reflux to obtain a Au colloid solution.

400 μL of a silver nitrate ($AgNO_3$) solution of a specific concentration (2, 4, 6, or 8 mmol/L) was added to the above Au@Cu_2O NPs solution. After stirring for 30 min, Ag nanocrystals attached to the surface of the Au@Cu_2O NPs, with the product denoted as Au@Cu_2O@Ag NPs.

2 mL of the Au@Cu_2O@Ag NPs dispersion was added to a 10 mL glass beaker, followed by slow addition of 1 mL cyclohexane under magnetic stirring at 300 r/min for 5 min to form a stable two-phase system. Subsequently, 1 cm^2 of Teflon tape was gently placed on the oil-water interface with tweezers. 1.5 mL of ethanol (inducer) was then injected into the aqueous phase through a syringe at a rate of 0.5 mL/min.

After the evaporation of cyclohexane at room temperature, a densely packed self-assembled film of Au@Cu_2O@Ag nanoarray was formed on Teflon tape.

2.3 Synthesis of the flexible EP/Au@Cu_2O@Ag/Teflon tape

After drying the prepared Au@Cu_2O@Ag/Teflon tape at 37 ℃, a specific volume of epoxy resin (EP) solution (E-51, with a viscosity of 1000-1500 mPa · s at 25℃) was drop-cast onto each piece of Au@Cu_2O@Ag/Teflon tape to achieve uniform encapsulation. Subsequently, the tapes were kept in a ventilated room for 24 h (temperature (25-30)℃, humidity 65%-70%), yielding EP/Au@Cu_2O@Ag/Teflon tape. Afterwards, the EP/Au@Cu_2O@Ag/Teflon tape was attached onto nitrile gloves to obtain a flexible SERS sensor.

After drying the prepared Au@Cu_2O@Ag/Teflon tape at 37 ℃, a specific volume of epoxy resin (EP) solution was drop-cast onto each piece of Au@Cu_2O@Ag/Teflon tape to achieve uniform encapsulation. Subsequently, the tapes were kept in a ventilated room for 24 h (temperature 25-30℃, humidity 65%-70%), yielding EP/Au@Cu_2O@Ag/Teflon tape. Afterwards, the EP/Au@Cu_2O@Ag/Teflon tape was attached onto nitrile gloves to obtain a flexible SERS sensor.

2.4 Spiked-sample preparation and SERS measurements

The pretreatment of spiked-samples including pepper, eggplant, oilseed rape, kiwifruit, grapes and pomelo was as follows: A 10^3 μmol/L bifenthrin standard solution was uniformly sprayed onto the surface of each sample to ensure homogeneous distribution using a calibrated sprayer. The spiked samples were then air-dried at room temperature (25 ± 2) ℃for 30 minutes to allow solvent evaporation, followed by storage at ambient conditions for 24 hours to simulate realistic pesticide residue scenarios. Subsequently, for analyte extraction, the prepared EP/Au@Cu_2O@Ag/Teflon tape was used to perform contact-based sampling: the prepared tape was gently applied to the spiked sample surfaces and reciprocally wiped with consistent pressure to ensure effective transfer of bifenthrin residues onto the SERS-active substrate.

SERS measurements were conducted directly on the analyte-coated sensor substrates using a portable Raman spectrometer. To ensure the consistency of measurement, three spatially separated locations were randomly selected for spectral acquisition.

3 Results and discussion

3.1 Optimization of the flexible EP/Au@Cu_2O@Ag/Teflon tape preparation

To optimize the thickness of the Ag shell size in the Au@Cu_2O@Ag nanoparticles, the amount of silver nitrate ($AgNO_3$) used in the synthesis of Ag NPs in the shell of Au@Cu_2O@Ag needed to be optimized. Specifically, 400 μL of different concentrations (2, 3, 4, 5, 6, 7, 8, 9 and 10 mmol/L) of silver nitrate ($AgNO_3$) solution were used to prepared Ag NPs to determine the ideal Ag shell size. For this purpose, 4-mercaptobenzonitrile (4-MBN) was used as the SERS probe. As shown in Fig. 1a and Fig. S1, the Raman intensity at 2231 cm^{-1} attributed to 4-MBN increased with the increasing concentrations of $AgNO_3$ solution up to a concentration of 6 mmol/L, then decreased at higher $AgNO_3$ concentrations. The optimal SERS activity at 6

mmol/L $AgNO_3$ likely arises from a well-defined, continuous Ag shell that maximizes localized surface plasmon resonance (LSPR) effects and promotes the formation of abundant SERS "hot spots". At higher concentrations, excessive Ag deposition may lead to particle aggregation, shell inhomogeneity, or damping of the plasmonic coupling, thereby reducing SERS efficiency. Consequently, 6 mmol/L of $AgNO_3$ solution was selected for the preparation of the Ag shell on the Au@Cu_2O@Ag NPs. Fig. 1b shows the UV-vis absorption spectrum for Au@Cu_2O@Ag NPs in a water-based solution. The Au@Cu_2O@Ag NPs exhibited an absorbance maximum at 452 nm. Following the addition of 1.5 mL of ethanol, a significant reduction in UV-vis absorbance at 452 nm was observed for the Au@Cu_2O@Ag NPs with different Ag shell thickness due to nanoarray formation. The efficiency of self-assembly was illustrated in Fig. S2 and calculated using the methodology in prior researches[34]. The results showed that when the concentration of $AgNO_3$ solution was 6 mmol/L, the self-assembly efficiency reached a maximum of ~79.6%.

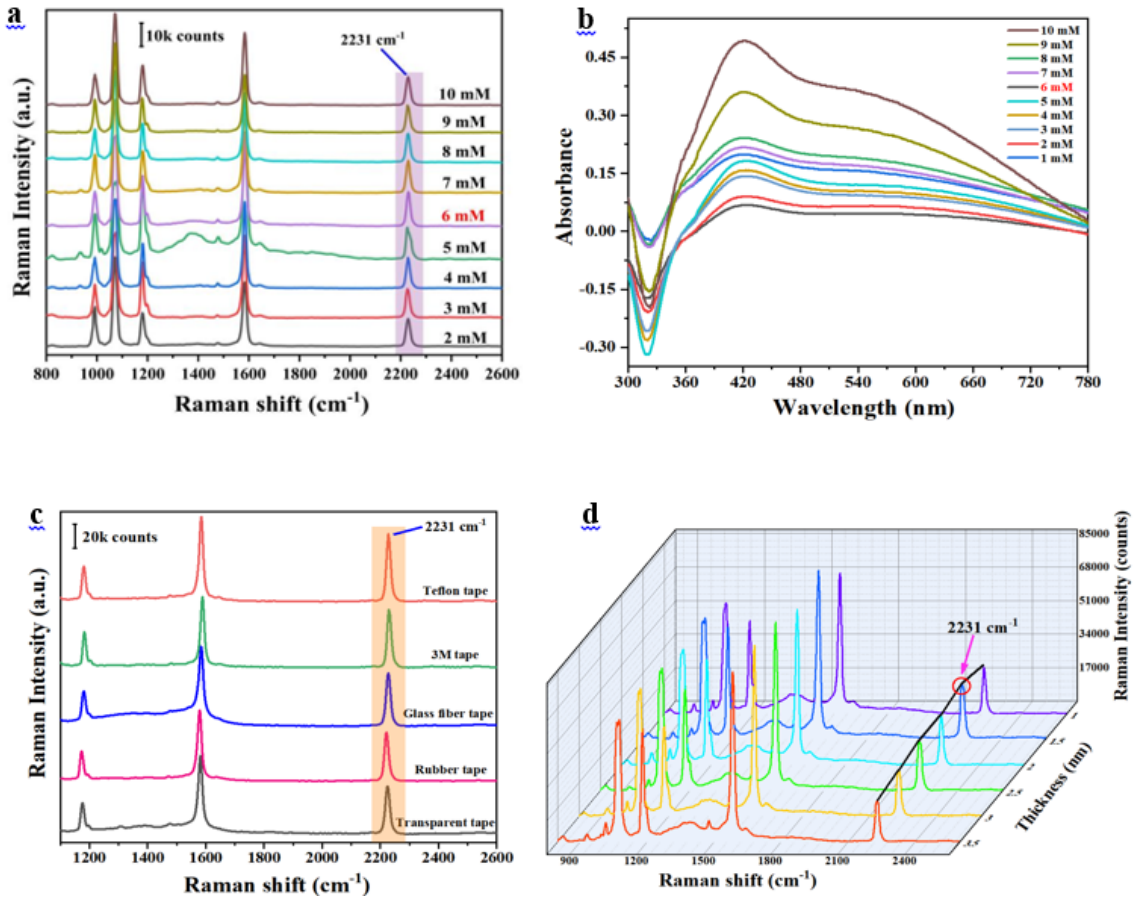

Fig. 1. (a) SERS spectra for Au@Cu_2O@Ag prepared with different sizes. The concentration of $AgNO_3$ used in the synthesis of the Ag NPs is indicated. (b) UV-Vis absorption spectra for Au@Cu_2O@Ag remaining in the aqueous phase after nanoarray formation. (c) SERS spectra for Au@Cu_2O@Ag/Teflon tape flexible SERS sensor prepared with different types of tape. (d) SERS spectra for EP/Au@Cu_2O@Ag/Teflon tape flexible SERS sensor with different thickness (1, 1.5, 2, 2.5, 3, 3.5 μL) of EP.

To investigate the effect of tape type of the performance of SERS substrate, different types of tape, including transparent tape, rubber tape, glass fiber tape, 3M tape and Teflon tape and were utilized to investigate their effects on SERS enhancement. Results indicated that the use of Teflon tape as the substrate provided the most significant SERS enhancement effect (Fig. 1c and Fig. S3). Thus, Au@Cu_2O@Ag/Teflon tape was used in subsequent experiments.

Subsequently, the effect of the thickness of epoxy resin solutions on the SERS enhancement of the Au@Cu_2O@Ag/Teflon tape on the SERS enhancement was systematically explored. As shown in Fig. 1d and Fig. S4, the Raman intensity at 2231 cm^{-1} reached its maximum when the thickness of epoxy resin was 1.5 nm. This enhancement is mainly ascribed to the concentrative effect of the hydrophobic epoxy layer on the 4-MBN solution. However, when the thickness exceeds 1.5 nm, the SERS enhancement of the prepared EP/Au@Cu_2O@Ag/Teflon tape experiences a decline. This phenomenon may be linked to obstruction of the molecule by a thick epoxy layer from the local electromagnetic field, leading to a drastic reduction of the Raman signal amplification effect[35].

3.2. Characterization of the flexible EP/Au@Cu_2O@Ag Teflon tape

Microscopic topography characterization of EP/Au@Cu_2O@Ag nanoarray Teflon tape surface was conducted using scanning electron microscopy (SEM). Fig. 2a presented the SEM image of Au@Cu_2O@Ag NPs without self-assembly, where the particles are severely stacked and distributed unevenly. As shown in Fig. 2b and 2c, the surface of EP/Au@Cu_2O@Ag nanoarray primarily consisted of tightly packed nanoparticles, showing the SERS substrate to have excellent uniformity. This significant difference in morphology between the nanoparticles with and without self-assembly demonstrates the success of the interface assembly.

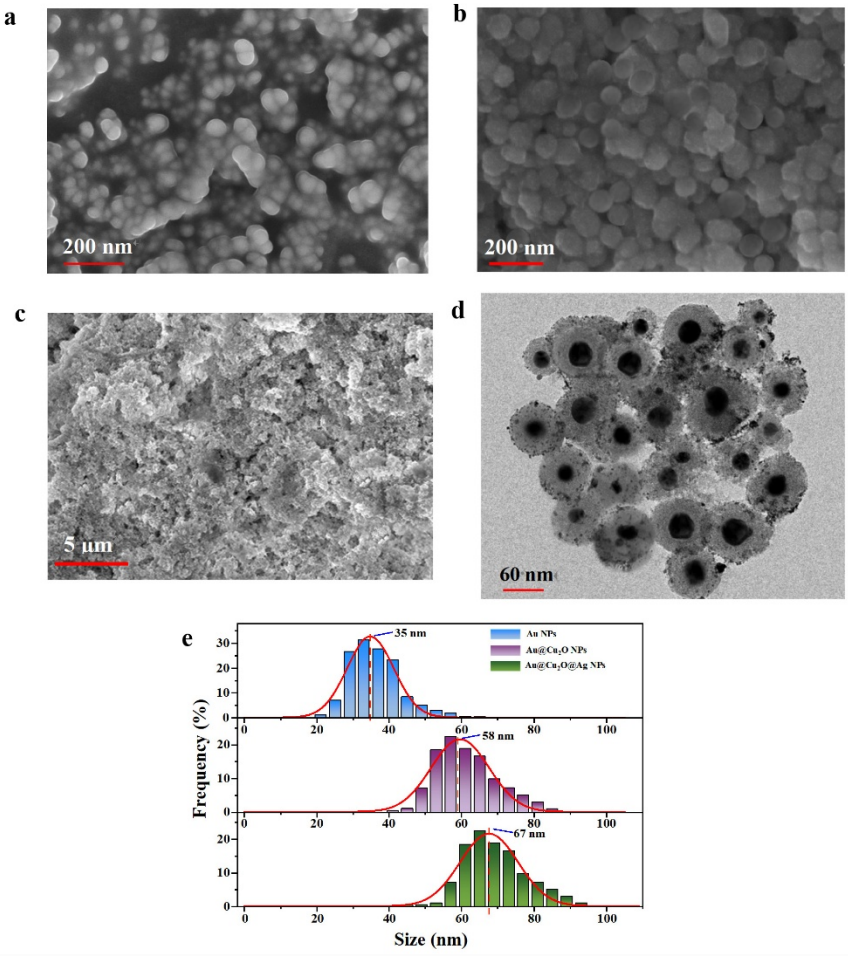

Fig. 2. (a) SEM images of EP/Au@Cu_2O@Ag NPs. (b) and (c) SEM images of EP/Au@Cu_2O@Ag/Teflon tape. (d) TEM image of EP/Au@Cu_2O@Ag/Teflon tape. (e) Dynamic light scattering particle size distributions for Au NPs, Au@Cu_2O@Ag NPs and EP/Au@Cu_2O@Ag/Teflon tape nanoarray.

High-resolution TEM analysis (Fig. 2d) confirmed the monodisperse core-shell architecture of Au@Cu_2O@Ag nanoarray, which exhibits a spherical geometry. The Au cores have a uniform size of about 35 nm. The Au@Cu_2O size range from 55-65 nm, while the Au@Cu_2O@Ag NPs size was 65-70 nm. High-resolution imaging further verified the successful attachment of Ag NPs (5-10 nm) onto the Au@Cu_2O surfaces to form Au@Cu_2O@Ag NPs size, demonstrating effective synthesis of a ternary nanostructure.

The hydrodynamic diameters of Au NPs, Au@Cu_2O NPs, and Au@Cu_2O@Ag NPs were quantitatively analyzed by dynamic light scattering (DLS). As revealed in Fig. 2e, the nanoparticles exhibited average hydrodynamic diameters of about 35 nm (Au NPs), 58 nm (Au@Cu_2O NPs), and 65 nm (Au@Cu_2O@Ag NPs), respectively, further verifying the successful construction of a ternary nanostructure with an ultrathin Ag shell layer (~5 nm). The result closely aligned with TEM findings.

The structural characteristics of the Au@Cu_2O@Ag nanoarray were analyzed by X-ray diffraction (XRD). Fig. 3a revealed distinct diffraction peaks at 38.1°, 44.1°, 64.4°, and 77.3°, which were assigned to the (111), (200), (220), and (311) planes of face-centered cubic (fcc) Ag, consistent with the reference pattern (JCPDS No. 04-0783). Additional peaks for fcc Au (JCPDS No. 04-0784) and cubic Cu_2O (JCPDS No. 78-2076) were observed at 44.4° (111) and 36.4° (111), respectively, confirming the coexistence of all three crystalline phases without any detectable impurities.

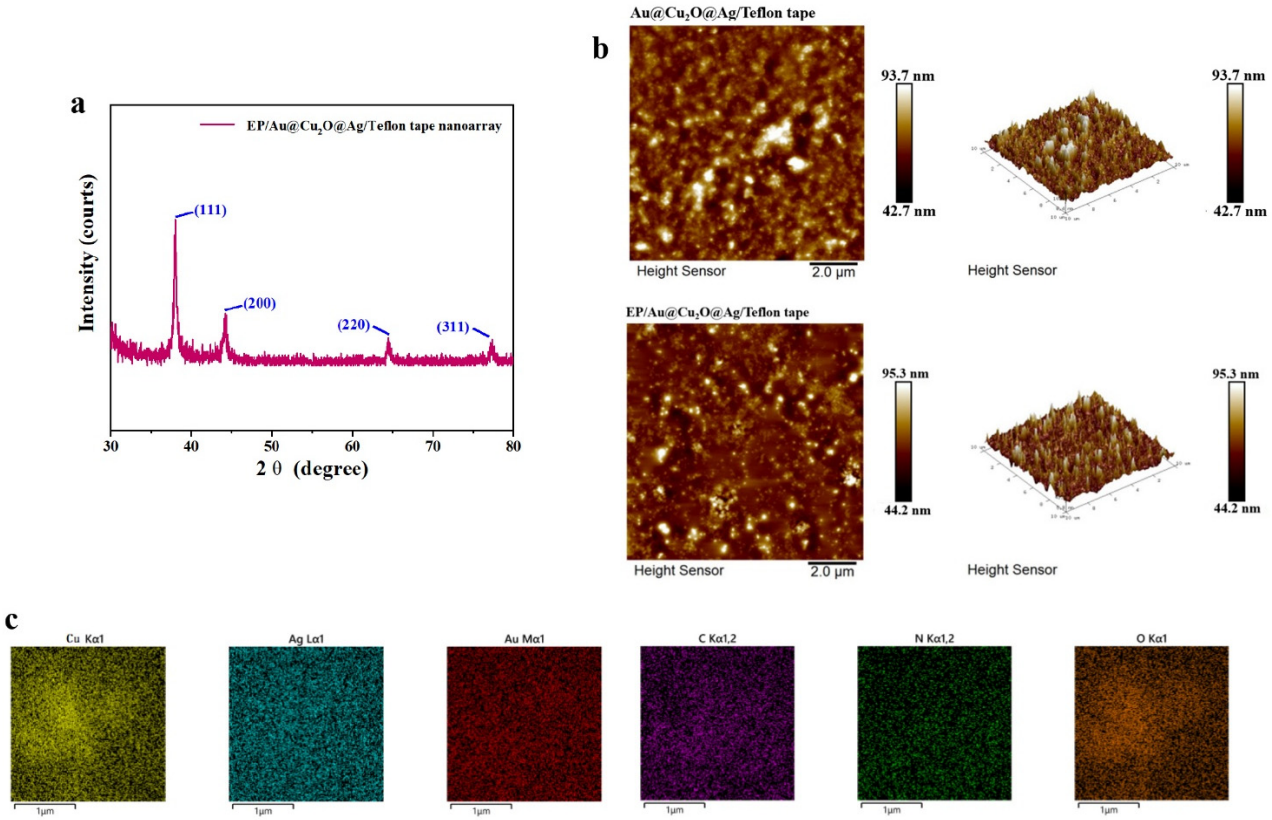

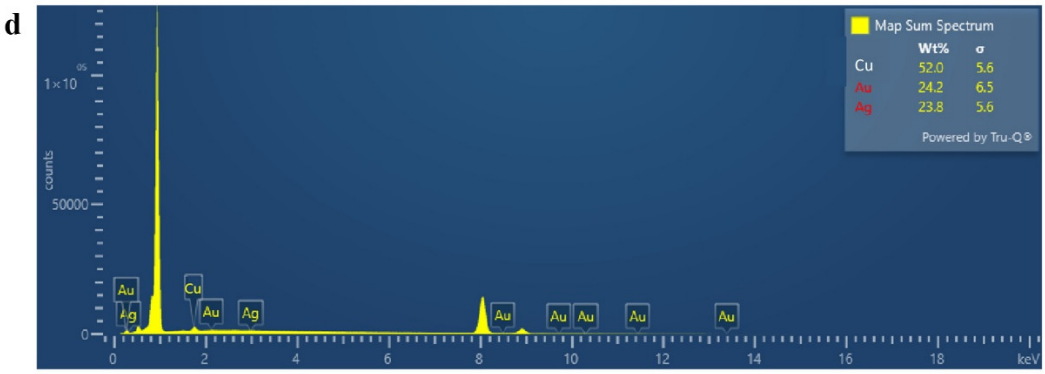

Fig. 3. (a) XRD pattern for EP/Au@Cu_2O@Ag/Teflon tape nanoarray. (b) Surface AFM map of Au@Cu_2O@Ag NPs and EP/Au@Cu_2O@Ag/Teflon tape nanoarray. (c) Elemental mapping images of the EP/Au@Cu_2O@Ag/Teflon tape nanoarray. (d) EDS spectra of the EP/Au@Cu_2O@Ag/Teflon tape nanoarray.

Atomic force microscopy (AFM) was employed to investigate the nanoscale topological features and surface homogeneity of Au@Cu_2O@Ag/Teflon tape and EP/Au@Cu_2O@Ag/Teflon tape. As illustrated in Fig. 3b, phase imaging in tapping mode corroborated the homogeneous distribution of components, with no discernible phase separation or interfacial discontinuities. The material exhibited an exceptionally smooth surface with a root mean square roughness (Rq) of (0.81 ± 0.11) nm and an average roughness (Ra) of (0.56 ± 0.09) nm, confirming the absence of agglomerations or microscale defects. Additionally, after coating with the EP layer, the overall thickness increased by approximately 1.5 nm, further attesting to the uniformity and conformality of the deposited layer. The ultra-smooth and homogeneous surface morphology was expected to minimize nonspecific adsorption and ensures reliable signal reproducibility during in situ pesticide detection. The results underscore the precision of EP/Au@Cu_2O@Ag/Teflon tape in achieving structurally optimized interfaces for high-performance flexible sensing applications.

Energy dispersive spectrometry (EDS) analysis of Au@Cu_2O@Ag NPs revealed the presence of C, O, N, Au, Ag and Cu in the sample, which was strong evidence for the successful preparation of Au@Cu_2O@Ag NPs (Fig. 3d). To further study the spatial distribution of elements, the EDS mapping of the Au@Cu_2O@Ag/Teflon tape nanoarray was also performed, as shown in Fig. 3c. It can be found that the Ag, Cu and Au elements were uniformly distributed on the Au@Cu_2O@Ag/Teflon tape surface.

3.3. Evaluation of the flexible EP/Au@Cu_2O@Ag/Teflon tape sensor

Bifenthrin shows characteristic Raman bands in the 500-1100 cm^{-1} region, with the most intense peak at 991 cm^{-1} being attributed to C-O-C stretching vibrations[36]. The 991 cm^{-1} peak was thus selected as the definitive spectral fingerprint for Bifenthrin and SERS sensor performance evaluation. The mechanical stability of the flexible SERS tape was systematically evaluated under cyclic bending and torsion (100 cycles) to simulate real-world operational stresses. As shown in Fig. 4a, the characteristic SERS intensity at 991 cm^{-1} retained 96.38% of its initial signal after repeated bending, attributable to the epoxy resin (EP)-enabled stress dissipation mechanism. The viscoelastic EP layer effectively redistributed localized shear forces during deformation, preventing dislocation or delamination of the Au@Cu_2O@Ag nanoarrays. Similarly, torsional testing resulted in only a 3.34% signal attenuation, confirming the substrate's resistance

to multidirectional mechanical perturbations (Fig. 4b). This exceptional stability stems from two synergistic factors: (1) covalent thiol-metal bonding between EP and nanoparticles, which suppresses interfacial slippage[37]; and (2) the intrinsic flexibility of Teflon tape minimizes strain transfer to the nanoarrays[38].

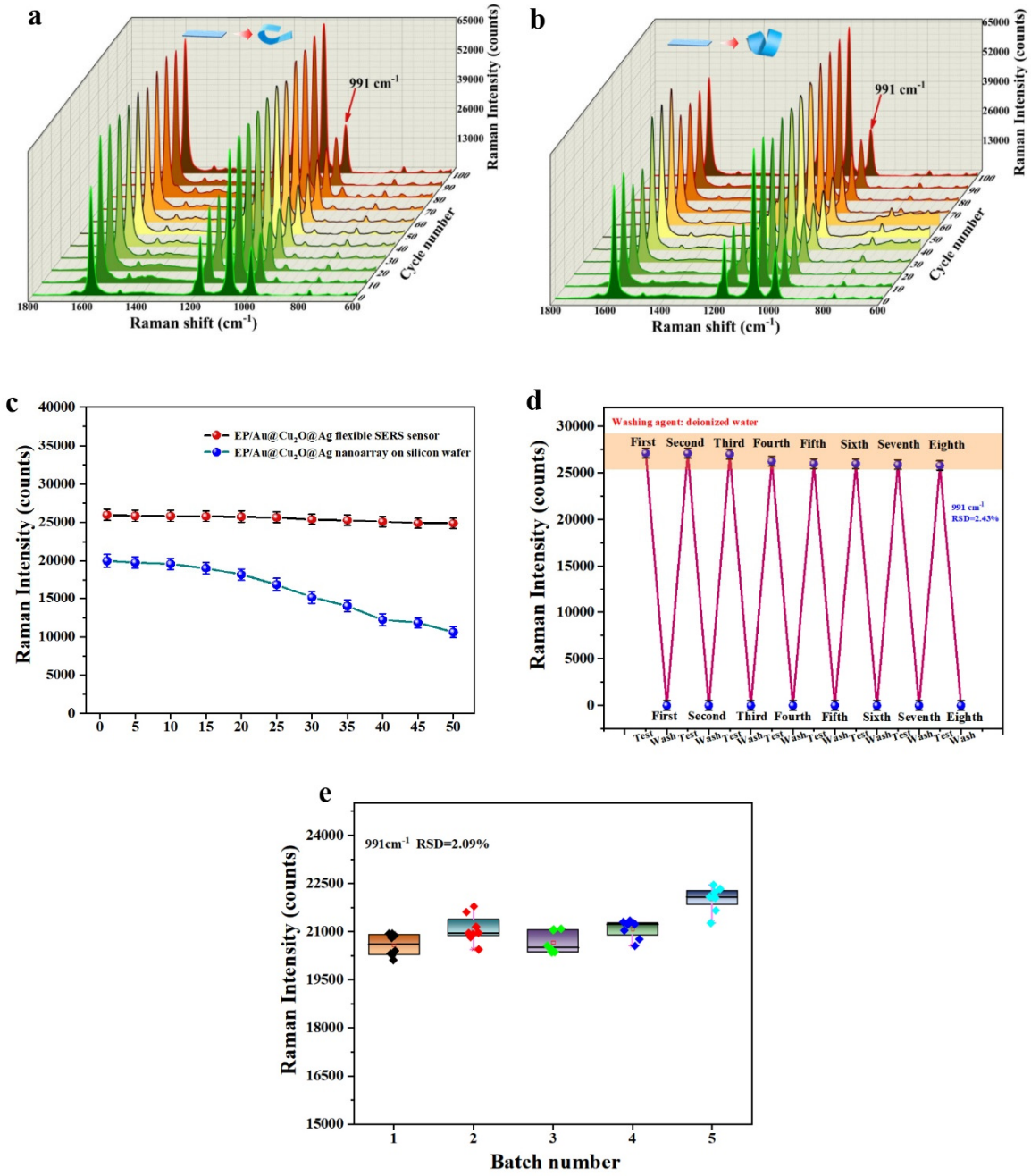

Fig. 4. Raman intensity at 991 cm^{-1} for bifenthrin (10^3 μmol/L) collected from the prepared flexible EP/Au@Cu_2O@Ag/Teflon tape during the (a) bending, (b) torsion tests for 100 cycles. (c) Raman intensity at 2231 cm^{-1} for flexible EP/Au@Cu_2O@Ag/Teflon tape after different storage times. (d) The relative SERS intensity of bifenthrin (10^3 μmol/L) was measured by the recovery test of the prepared SERS sensor using deionized water as the washing agent. (e) Box-whisker plots of Raman intensity at 991 cm^{-1} for 5 batches of EP/Au@Cu_2O@Ag/Teflon tape, with 40 randomly selected spots per batch.

To evaluate long-term storage stability, the SERS intensity at 991 cm^{-1} of the flexible EP/Au@Cu_2O@Ag/Teflon tape and EP/Au@Cu_2O@Ag nanoarray-decorated silicon wafer was systematically compared at varying storage times (0-50 days). As shown in Fig. 4c, the comparison revealed that the flexible tape exhibited exceptional stability, with only a 4.27% signal decrease over 50 days,

significantly outperforming the EP/Au@Cu_2O@Ag nanoarray on silicon wafer (47.05% intensity loss). These results demonstrate its suitability for long-term field deployment and batch production storage, addressing a critical limitation in conventional rigid SERS substrates.

The reusability of the flexible EP/Au@Cu_2O@Ag/Teflon tape was systematically evaluated through eight consecutive cleaning-reuse cycles (Fig. 4d). After each detection cycle, the material was subjected to a simple washing process with deionized water. Remarkably, the material maintained a high level of performance after eight reuses. The Raman intensity for bifenthrin detection showed only a slight decrease, with a relative standard deviation (RSD) of less than 2.43% across all eight cycles. The above results proved that the flexible EP/Au@Cu_2O@Ag/Teflon tape exhibits outstanding reusability, making it a promising candidate for long-term and cost-effective pesticide residue detection in the foods.

To investigate the reproducibility of the developed flexible EP/Au@Cu_2O@Ag/Teflon tape, SERS intensity at 991 cm^{-1} was measured from 40 randomly selected spots in 5 batches of the material. As shown in Fig. 4f, the interquartile ranges (IQRs) in the boxplots are relatively narrow, the data points show small deviations from the medians, and there are no significant outliers, indicating low variability within and between batches. Additionally, the material demonstrated exceptional batch-to-batch and spatial reproducibility, as evidenced by a low relative standard deviation (RSD = 3.95%) in SERS intensity at 991 cm^{-1}.It can be concluded that the flexible EP/Au@Cu_2O@Ag/Teflon tape exhibits superior reproducibility.

To evaluate the transfer efficiency of the EP/Au@Cu_2O@Ag/Teflon tape for bifenthrin, we compared the SERS intensity at 991 cm^{-1} from two sampling methods: (1) direct spraying of a 10^3 μM bifenthrin standard solution onto the tape, and (2) wiping the same solution from actual sample surfaces using the tape. As shown in Fig. 5a, the average transfer efficiency reached 98.96%, demonstrating high analyte collection capability. Furthermore, uniformity tests across 20 random points showed a relative standard deviation (RSD) below 5.20% (Figure 5b), confirming consistent sampling performance. The high transfer efficiency and uniformity ensure detection reliability and contribute to a lower detection limit.

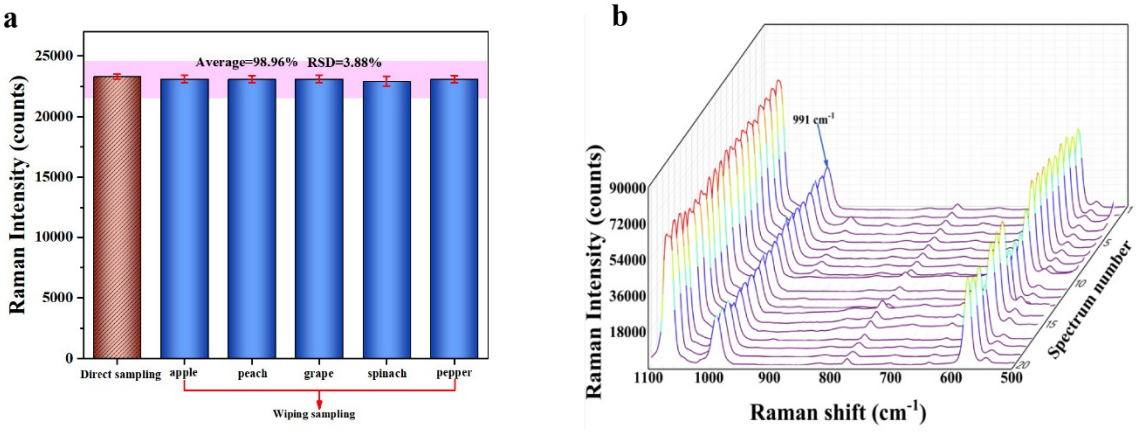

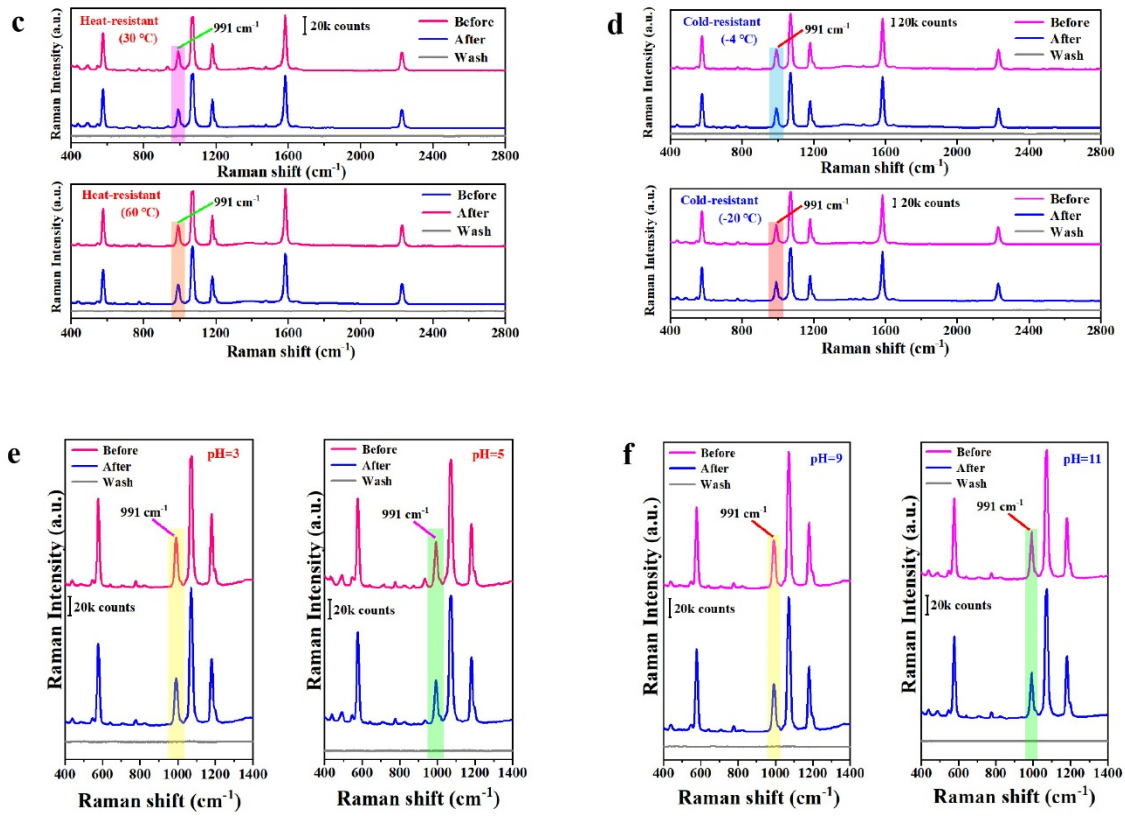

Fig. 5. (a) Raman intensity of direct and wiping sampling of apple, peach, grape, spinach, pepper. (b) SERS intensity at 991 cm^{-1} from 40 randomly selected spots in 6 batches of Ag@4-MBN@Ag nanoarrays. (c) SERS spectra for flexible EP/Au@Cu_2O@Ag/Teflon tape during temperature tolerance test (heat resistant). (d) SERS spectra for flexible EP/Au@Cu_2O@Ag/Teflon tape during temperature tolerance test (cold resistant). (e) and (f) SERS spectra for flexible EP/Au@Cu_2O@Ag/Teflon tape during pH tolerance test.

To ensure reliable operation in extreme environments, the temperature tolerance of the prepared SERS substrate was systematically evaluated. As shown in Fig. 5c and Fig. S5, the flexible EP/Au@Cu_2O@Ag/Teflon tape demonstrated exceptional thermal stability. At 30℃ and 60℃, Raman intensity remained consistent (< 5% variation), attributed to EP crosslinked network that suppresses nanoparticle aggregation and maintains plasmonic activity. Similarly, cryogenic testing (-4℃ and -20℃) revealed no significant signal degradation (< 3% variation), enabled by the low-temperature flexibility of Teflon and the ice-resistant properties of EP (Fig. 5d and Fig. S6). The good performance of the constructed material under extreme temperatures validates its suitability for field applications in diverse climatic conditions.

To investigate the sensors applicability in acidic/alkaline food surfaces, its pH tolerance was systematically investigated across acidic and alkaline environments. As shown in Fig. 5e and 5f, the material demonstrated robust pH tolerance across acid and alkaline environments, retaining > 94% of its initial SERS intensity at 991 cm^{-1} after 2 h exposure. In acid media (pH=3 or pH=5), the hydrophobicity of Teflon tape prevented acid-induced nanoparticle aggregation, while the amine groups of EP neutralized protonation effects. In alkaline media (pH=9 or pH=10), the crosslinked EP matrix shielded Au@Cu_2O@Ag nanostructures from hydroxyl corrosion, preserving plasmonic activity. These results demonstrate

EP/Au@Cu_2O@Ag/Teflon tape significantly outperforms conventional SERS substrates, confirming the material was suitable for analyzing acid/alkaline food surfaces.

3.4. SERS enhancement performance of the flexible EP/Au@Cu_2O@Ag/Teflon tape

The SERS enhancement capability of the EP/Au@Cu_2O@Ag/Teflon tape flexible SERS sensor was systematically investigated using 4-mercaptobenzonitrile (4-MBN) as a Raman reporter. As shown in Fig. S7, the characteristic C≡N stretching vibration of 4-MBN at 2231 cm^{-1} exhibited progressive signal amplification across three configurations: Au@Cu_2O NPs (15025 counts), Au@Cu_2O@Ag NPs (22536 counts), and the flexible EP/Au@Cu_2O@Ag/Teflon tape (32599 counts). The results demonstrated that the flexible EP/Au@Cu_2O@Ag/Teflon tape benefitted from a ternary plasmonic heterostructure and abundant "hot-spots".

3.5. Establishment of the flexible EP/Au@Cu_2O@Ag/Teflon tape SERS sensor method for bifenthrin detection

To evaluate the effect of wiping repetitions on the sensing performance, the EP/Au@Cu_2O@Ag/Teflon tape flexible SERS sensor was systematically tested with bifenthrin samples under wiping cycles ranging from 1 to 10. For each wiping cycle, the round-bottomed flask was used to simulate the actual sample, and a certain concentration of bifenthrin standard solution was sprayed on the flask surface. Subsequently, the EP/Au@Cu_2O@Ag/Teflon tape was manually dragged across the round-bottomed flask surfaces, simulating on-site sampling conditions. Thanks very much for your insightful comment. In response, we have supplemented the mechanistic justification for the wipe-cycle optimization in the revised manuscript. As detailed on page 10 (line 180), page 17 (line 336), and supported by Fig. 1a, 1b and Fig. S2, the observed trend in SERS intensity can be attributed to the cumulative transfer of analyte molecules from the contaminated surface to the SERS-active substrate with repeated wiping. As shown in Fig. 6a and 6b, the SERS intensity at 991 cm^{-1} increased progressively with wiping frequency, reaching its maximum at 7 cycles before stabilizing. The observed increase in SERS intensity with repeated wiping (from 1 to 7 cycles) is attributed to the progressive transfer of bifenthrin molecules from the contaminated surface to the SERS substrate. Each wiping cycle enhances the adsorption of analyte molecules onto the sensing surface, thereby improving the overall collection efficiency. The signal saturation beyond 7 cycles suggests that the majority of accessible analyte molecules have been effectively captured by the substrate, with additional cycles providing no significant further enhancement. This optimal cycle number represents a balance between maximal signal acquisition and operational practicality, ensuring high detection performance during real-world pesticide sampling applications[39-40]. Consequently, 7 wiping cycles were adopted as the optimal condition for subsequent experiments.

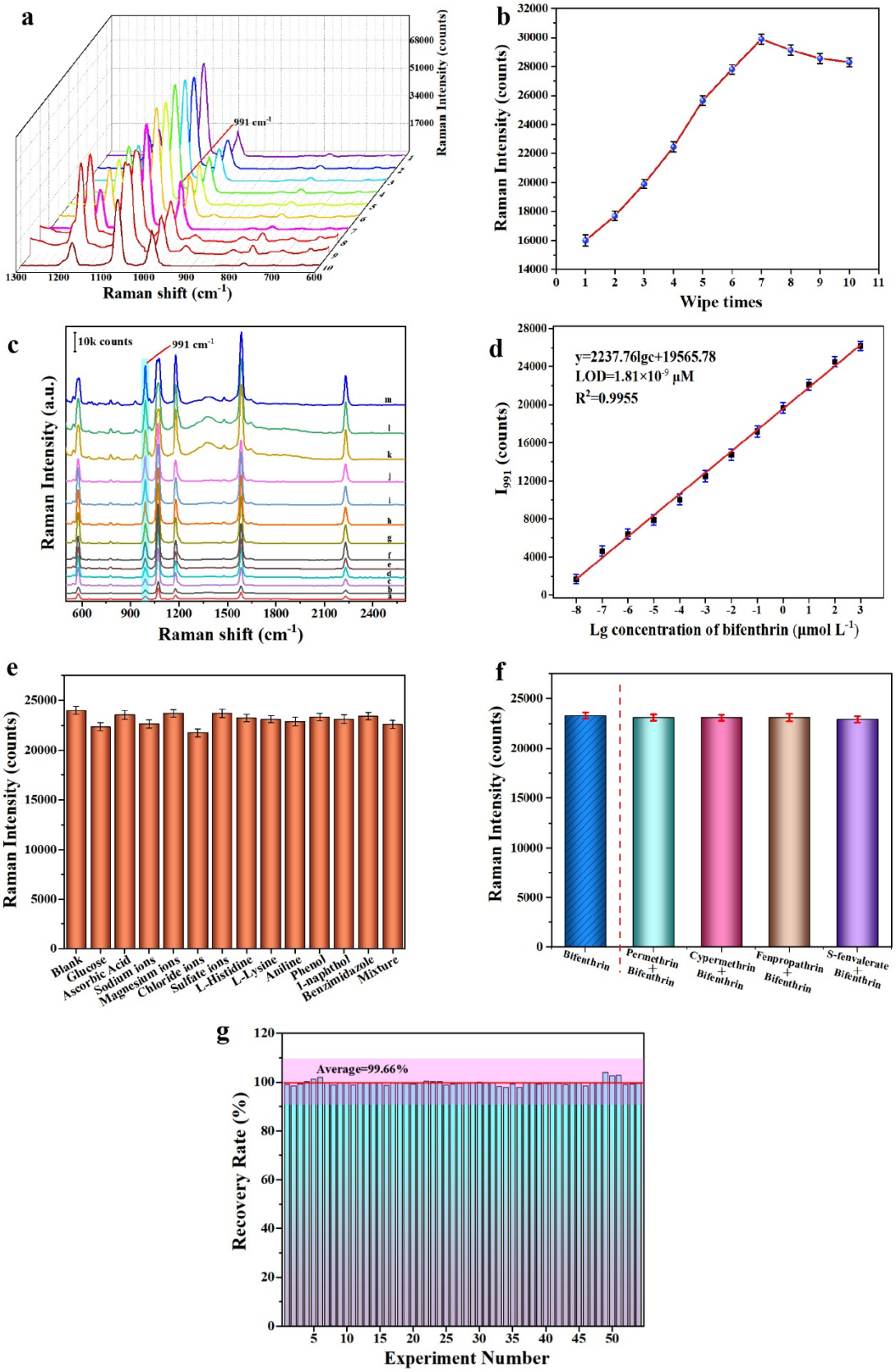

Fig. 6. (a) Raman intensity at 991 cm^{-1} for bifenthrin with different wipe times. (b) Plot of Raman intensity at 991 cm^{-1} versus incubation time. (c) SERS spectra for bifenthrin at different concentrations, a - m: 10^{-8}, 10^{-7}, 10^{-6}, 10^{-5}, 10^{-4}, 10^{-3}, 10^{-2}, 10^{-1}, 1, 10, 10^{2}, 10^{3} μmol/L, respectively. (d) Linear relationship between I_{991} and the logarithm of the bifenthrin concentration over the range 10^{-8}-10^{3} μmol/L. (e) Raman intensity at 991 cm^{-1} for the EP/Au@Cu_2O@Ag/Teflon tape flexible SERS sensor in the presence of different possible interferents. (f) Raman intensity at 991 cm^{-1} for the EP/Au@Cu_2O@Ag/Teflon tape flexible SERS sensor in the presence of different pesticides (permethrin, cypermethrin, fenpropathrin, S-fenvalerate). (g) Recovery rate of 50 experiments, with an average of 99.66%.

A flexible SERS sensing sensor was developed for rapid bifenthrin residue analysis, following the optimized testing conditions. For this method, the round-bottomed flask was still used to simulate the actual sample. The method involved uniformly spraying bifenthrin standard solutions onto round-bottom flask surfaces, followed by direct sampling using the EP/Au@Cu_2O@Ag/Teflon tape flexible SERS sensor (Fig. S8). Following the sampling procedure, the EP/Au@Cu_2O@Ag/Teflon tape flexible SERS sensor was subjected to spectral acquisition under optimized conditions. As shown in Fig. 6c, the characteristic Raman intensity at 991 cm^{-1} (I_{991}) demonstrated a logarithmic correlation with bifenthrin concentrations ranging from 10^{-8} to 10^3 μmol/L. Quantitative analysis revealed a strong linear correlation (Fig. 6d) between I_{991} and the logarithm of bifenthrin concentration (lg c), fitted as $y = 2237.76 \lg c + 19565.78$ ($R^2 = 0.9955$). The method demonstrated ultrahigh sensitivity with a calculated limit of detection (LOD, S/N = 3) of 1.81×10^{-9} μmol/L.

Table S1 presents a comparison of the analytical performance between the developed EP/Au@Cu_2O@Ag/Teflon tape flexible SERS sensor and previously reported sensors for bifenthrin detection. In contrast to other sensing approaches, the fabricated sensor demonstrates two key advantages: a lower LOD and a broader linear response range. Additionally, this method combines efficient one-step sampling with on-site detecting, offering a practical solution for monitoring bifenthrin residues in foods.

3.6. Evaluation of the flexible EP/Au@Cu_2O@Ag/Teflon tape SERS sensor method

The interference resistance of the method was rigorously evaluated via the introduction of interferents (e.g., inorganic ions, organic compounds, aniline, phenol, 1-naphthol and benzimidazole) at a 10^2-fold concentration into 10^3 μmol/L bifenthrin solutions (Fig. 6e and Fig. S9). These interferents were specifically selected as they are commonly present in food matrices (e.g., inorganic ions like sodium and potassium ions are ubiquitous in vegetables and fruits; organic compounds such as glucose and amino acids are abundant in various food samples; aniline, phenol, 1-naphthol and benzimidazole are frequently detected as residues or metabolites in agricultural products). Remarkably, the SERS intensity at 991 cm^{-1} showed negligible variation in the presence of any of these possible interferants. The superior anti-interference of the prepared sensor ensures reliable detection in multicomponent food samples.

The selectivity of the substrate was evaluated by comparing the SERS intensity of bifenthrin alone and in the presence of other common pesticides (such as fenthion, fenvalerate, fipronil, and S-fenvalerate). As shown in Fig. 6f, the SERS intensity of bifenthrin at 991 cm^{-1} remained unaffected by equiconcentrated interfering pesticides, demonstrating the high selectivity of EP/Au@Cu_2O@Ag/Teflon tape for bifenthrin. This specificity is attributed to the fact that this SERS substrate can only recognize the characteristic peak at 991 cm of bifenthrin, and other similar substances have no effect on this peak. This specificity arises from the ability of the SERS substrate to exclusively recognize the characteristic peak of bifenthrin at 991 cm^{-1}, with no interference from other similar substances on this peak.

The accuracy of the EP/Au@Cu_2O@Ag/Teflon tape flexible SERS sensor method was examined by spiking known quantities of bifenthrin into pepper, eggplant, oilseed rape, kiwi fruit, grapes and pomelo. As

shown in Table 1, the recovery rates ranged from 94.18% to 104.53% with low RSDs of 0.33%-3.34%). Additionally, the recovery rates are highly concentrated around 100%, with an average of 99.66% and the data exhibit minimal fluctuations and no obvious outliers (Fig. 6g). This indicates that the reliability of the constructed SERS sensor for rapid, on-site quantification of bifenthrin in real food samples.

Table 1. Recoveries of bifenthrin in spiked food samples detected by the prepared SERS sensor.

Samples	Original level ($\times 10^{-4}$ μg g^{-1})	Added level ($\times 10^{-4}$ μg g^{-1})	Found level ($\times 10^{-4}$ μg g^{-1}, ± SD)	Recovery (±RSD, %)
Pepper	0	1.00	0.99 ± 0.05	99.00 ± 2.01
		5.00	5.11 ± 0.02	102.20 ± 1.05
		10.00	9.79 ± 0.14	97.90 ± 1.11
Eggplant	0	1.00	0.97 ± 0.11	97.00 ± 2.82
		5.00	4.98 ± 1.99	99.60 ± 1.73
		10.00	9.99 ± 0.31	99.90 ± 2.77
Oilseed rape	0	1.00	0.99 ± 1.11	99.00 ± 3.22
		5.00	4.89 ± 0.27	97.80 ± 1.97
		10.00	10.02 ± 0.35	100.02 ± 2.03
Kiwi fruit	0	1.00	0.98 ± 1.17	98.00 ± 3.12
		5.00	4.99 ± 0.31	99.80 ± 1.97
		10.00	9.96 ± 2.44	99.60 ± 2.03
Grapes	0	1.00	0.99 ± 2.03	99.00 ± 1.78
		5.00	4.88 ± 0.55	97.60 ± 2.13
		10.00	9.96 ± 0.61	99.60 ± 3.01
Pomelo	0	1.00	1.03 ± 1.13	98.00 ± 3.34
		5.00	5.21 ± 0.22	104.20 ± 0.33
		10.00	9.98 ± 2.44	99.80 ± 2.03

Additionally, the practical applicability of the EP/Au@Cu_2O@Ag/Teflon tape flexible SERS sensor method was rigorously validated through comparative analysis with GC method for bifenthrin detection in real food samples (tomato, cauliflower, cucumber, Chinese cabbage, strawberry, blueberry, orange, apple, pear). As presented in Table 2, bifenthrin concentrations determined by the glove sensor (range: 1.32-5.41 μg/kg) exhibited statistically insignificant differences ($P > 0.05$) from GC results (1.30-5.26 μg/kg). Notably, the glove SERS sensor achieved these results without sample pretreatment, contrasting with the laborious extraction protocols required for GC analysis. No significant differences were found between the results of the prepared sensor and GC method, demonstrating the flexible SERS sensor can be applied for the rapid, on-site bifenthrin detection in real samples.

Table 2 Performance comparison of the developed SERS sensor method and a GC method for the detection of bifenthrin in food samples.

Samples	Found level by the developed SERS sensor method ($\times 10^{-2}$ μg g^{-1})	Found level by GC ($\times 10^{-2}$ μg g^{-1})
Tomato	2.87[a]	2.81[a]
Cauliflower	2.22[a]	2.17[a]
Cucumber	4.62[a]	4.58[a]
Chinese cabbage	3.19[a]	3.15[a]
Strawberry	2.87[a]	2.81[a]
Blueberry	5.41[a]	5.26[a]
Orange	1.32[a]	1.30[a]
Apple	1.89[a]	1.79[a]
Pear	3.02[a]	3.01[a]

Note: "a" indicated that there was no discernible difference between the data ($P > 0.05$).

4. Conclusions

In summary, a flexible and reusable SERS sensor was successfully developed for rapid, nondestructive detection of bifenthrin in complex food matrices. The Teflon substrate facilitated uniform nanoarrays assembly with high-density "hot spots", while EP ensured mechanical robustness and oxidative stability, enabling a wide linear range with low LOD for bifenthrin detection in practical food samples. Notably, the developed flexible EP/Au@Cu_2O@Ag/Teflon tape SERS sensor could enable one-step, pretreatment-free sampling on irregular surfaces, delivering on-site results within 3 minutes. This work establishes a paradigm for flexible SERS sensors in food safety monitoring, offering a practical solution for rapid pesticide screening without laboratory dependencies. For further work, integrating this sensor with integrate smartphone-based analysis could enhance field operability, while optimizing the nanoarray structure may improve sensitivity for ultra-trace analyte detection.

Conflict of Interest Statement

We declare that we have no conflict of interest.

Acknowledgement

This work was financially supported by the Key R&D Program of Shandong Province, China (2023CXGC010712). GINW acknowledges funding support from the MacDiarmid Institute for Advanced Materials and Nanotechnology.

References

[1] W. Park, S. Park, W. Lim, G. Song, Bifenthrin reduces pregnancy potential via induction of oxidative stress in porcine trophectoderm and uterine luminal epithelial cells, *Science of the Total Environment*. 784 (2021) 147143. https://doi.org/10.1016/j.scitotenv.2021.147143.

[2] M. Dai, X. Dong, Y. Yang, Y. Wu, L. Chen, C. Jiang, Z. Guo, T. Yang, Mechanistic insight into the impact of interaction between goethite and humic acid on the photooxidation and photoreduction of bifenthrin, *Environmental Research*. 252 (2024) 118779. https://doi.org/10.1016/j.envres.2024.118779.

[3] M.J. Wolansky, K.L. McDaniel, V.C. Moser, K.M. Crofton, Influence of dosing volume on the neurotoxicity of bifenthrin, *Neurotoxicology and Teratology*. 29 (2007) 377-384. https://doi.org/10.1016/j.ntt.2007.01.007.

[4] F. Mukhtar, K. Jilani, I. Bibi, Z. Mushataq, M.A. Bari Khan, M. Fatima, Stimulation of erythrocyte membrane blebbing by bifenthrin induced oxidative stress, *Dose-Response*. 20 (2022) 15593258221076710. https://doi.org/10.1177/15593258221076710.

[5] K. Shi, L. Li, W. Li, L. Yuan, F. Liu, Chronic and acute risk assessment of human exposed to novaluron-bifenthrin mixture in cabbage, *Environmental Monitoring and Assessment*. 188 (2016) 528. https://doi.org/10.1007/s10661-016-5536-4.

[6] S.S. Alhewairini, R.M. Abd El-Hamid, N.S. Ahmed, S.B. Abdel Ghani, O.I. Abdallah, Bifenthrin residues in table grapevine: method optimization, dissipation and removal of residues in grapes and grape leaves, *Plants*. 13 (2024) 1695. https://doi.org/10.3390/plants13121695.

[7] R. Chaudhary, R. Singh, M. Singh, N.K. Mogha, P. Kumari, G. Paliwal, P.P. Singh, M. Das, LC-MS/MS method for the simultaneous quantification of pyriproxyfen and bifenthrin and their dissipation kinetics under field conditions in chili and brinjal, *Journal of Food Science*. 87 (2022) 1331-1341. https://doi.org/10.1111/1750-3841.16070.

[8] J.M. Gonçalves Barbosa, A.F. Machado Botelho, R.H. Santana da Silva, S.S. Ferreira de Almeida, E.R. Ferreira, L. Caetano David, D. Alves Fortuna Lima, T. Cavalcante E Silva, P.H. Jorge da Cunha, N. Roberto Antoniosi Filho, Identification of cattle

poisoning by bifenthrin via earwax analysis by HS/GC-MS, *Biomedical Chromatography*. 35 (2021) e5017. https://doi.org/10.1002/bmc.5017.

[9] J. Yao, X. Xu, L. Liu, H. Kuang, C. Xu, Gold nanoparticle-based immunoassay for the detection of bifenthrin in vegetables, *Food Additives & Contaminants: Part A*. 39 (2022) 531-541. https://doi.org/10.1080/19440049.2021.2020909.

[10] S. Bhandari, B. Sen, S. Khatua, L.R. Singh, V.S. Parihar, M. Mahato, Ruthenium complex based nanocomposite film with enhanced and selective electrochemical sensing of bifenthrin pesticide, *RSC Advances*. 14 (2024) 29542-29558. https://doi.org/10.1039/d4ra04188g.

[11] L. Zhang, W. Cai, W.Y. Chen, L. Zhang, K. Hu, Y.Q. Guan, Synthesis of AzPhchitosan-bifenthrin-PVC to protect cables against termites, *Carbohydrate Polymers*. 139 (2016) 50-60. https://doi.org/10.1016/j.carbpol.2015.11.075.

[12] T. Dong, L. Lin, Y. He, P. Nie, F. Qu, S. Xiao, Density functional theory analysis of deltamethrin and its determination in strawberry by surface enhanced Raman spectroscopy, *Molecules*. 23 (2018) 1458. https://doi.org/10.3390/molecules23061458.

[13] A.N. Hidayah, D. Triyono, Y. Herbani, R. Saleh, Liquid surface-enhanced Raman spectroscopy (SERS) sensor-based Au-Ag colloidal nanoparticles for easy and rapid detection of deltamethrin pesticide in brewed tea, *Crystals*. 12 (2022) 24. https://doi.org/10.3390/cryst12010024.

[14] T. Yaseen, H.B. Pu, D.W. Sun, Functionalization techniques for improving SERS substrates and their applications in food safety evaluation: a review of recent research trends, *Trends in Food Science & Technology*. 72 (2018) 162-174. https://doi.org/10.1016/j.tifs.2017.12.012.

[15] A. Matikainen, T. Nuutinen, T. Itkonen, S. Heinilehto, J. Puustinen, J. Hiltunen, J. Lappalainen, P. Karioja, P. Vahimaa, Atmospheric oxidation and carbon contamination of silver and its effect on surface-enhanced Raman spectroscopy (SERS), *Scientific Reports*. 6 (2016) 37192. https://doi.org/10.1038/srep37192.

[16] T. Wu, Y. Kou, H. Zheng, J. Lu, N.R. Kadasala, S. Yang, C. Guo, Y. Liu, M. Gao, A novel Au@Cu_2O-Ag ternary nanocomposite with highly efficient catalytic performance: towards rapid reduction of methyl orange under dark condition, *Nanomaterials*. 10 (2019) 48. https://doi.org/10.3390/nano10010048.

[17] S.Y. Gezgin, A. Kepceoğlu, Y. Gündoğdu, S. Zongo, A. Zawadzka, H.Ş. Kiliç, B. Sahraoui, Effect of Ar gas pressure on LSPR property of Au nanoparticles: comparison of experimental and theoretical studies, *Nanomaterials*. 10 (2020) 1071. https://doi.org/10.3390/nano10061071.

[18] M. Ge, P. Li, G. Zhou, S. Chen, W. Han, F. Qin, Y. Nie, Y. Wang, M. Qin, G. Huang, S. Li, Y. Wang, L. Yang, Z. Tian, General surface-enhanced Raman spectroscopy method for actively capturing target molecules in small gaps, *Journal of the American Chemical Society*. 143 (2021) 7769-7776. https://doi.org/10.1021/jacs.1c02169.

[19] L. Tian, M. Su, F. Yu, Y. Xu, X. Li, L. Li, H. Liu, W. Tan, Liquid-state quantitative SERS analyzer on self-ordered metal liquid-like plasmonic arrays, *Nature Communications*. 9 (2018) 3642. https://doi.org/10.1038/s41467-018-05920-z.

[20] G.H. Kim, J. Son, J.M. Nam, Advances, challenges, and opportunities in plasmonic nanogap-enhanced Raman scattering with nanoparticles, *ACS Nano*. 19 (2025) 2992-3007. https://doi.org/10.1021/acsnano.4c14557.

[21] X. Wei, W. Song, Y. Fan, Y. Sun, Z. Li, S. Chen, J. Shi, D. Zhang, X. Zou, X. Xu, A SERS aptasensor based on a flexible substrate for interference-free detection of carbendazim in apple, *Food Chemistry*. 431 (2024) 137120. https://doi.org/10.1016/j.foodchem.2023.137120.

[22] S. Sloan-Dennison, G.Q. Wallace, W.A. Hassanain, S. Laing, K. Faulds, D. Graham, Advancing SERS as a quantitative technique: challenges, considerations, and correlative approaches to aid validation, *Nano Convergence*. 11 (2024) 33. https://doi.org/10.1186/s40580-024-00443-4.

[23] X. Li, H. Li, K. Zhao, H. Wang, Z. Zhang, L. Huang, H.J. Niu, Z.S. Yang, C. Wang, Biomimetic flexible SERS substrates replicated from cicada wings for portable in situ detection, *Optical Materials*. 149 (2024) 114801. https://doi.org/10.1016/j.optmat.2023.114801.

[24] L. Xie, H. Zeng, J. Zhu, Z. Zhang, H.-B. Sun, W. Xia, Y. Du, State of the art in flexible SERS sensors toward label-free and onsite detection: from design to applications, *Nano Research*. 15 (2022) 4374-4394. https://doi.org/10.1007/s12274-021-4017-4.

[25] T.T. Pan, D.W. Sun, H. Pu, Q. Wei, Simple approach for the rapid detection of alternariol in pear fruit by surface-enhanced Raman scattering with pyridine-modified silver nanoparticles, *Journal of Agricultural and Food Chemistry*. 66 (2018) 2180-2187. https://doi.org/10.1021/acs.jafc.7b05664.

[26] L. Li, W.S. Chin, Rapid fabrication of a flexible and transparent Ag nanocubes@PDMS film as a SERS substrate with high performance, *ACS Applied Materials & Interfaces*. 12 (2020) 37538-37548. https://doi.org/10.1021/acsami.0c07178.

[27] S.Z. Oo, R.Y. Chen, S. Siitonen, V. Kontturi, D.A. Eustace, J. Tuominen, S. Aikio, M.D. Charlton, Disposable plasmonic plastic SERS sensor, *Optics Express*. 21 (2013) 18484-18491. https://doi.org/10.1364/OE.21.018484.

[28] T. Zhang, X. Li, D. Liu, J. An, M. Zhang, J.H. Li, C. Jiang, Plasmonic AgNPs reinforced flexible hydrogel surface-enhanced Raman scattering (SERS) sensor for in-situ detection of curved samples, *Chemical Engineering Journal*. 494 (2024) 153082. https://doi.org/10.1016/j.cej.2024.153082.

[29] S. Columbus, K. Daoudi, K. Ramachandran, M. Shameer, H.H. Kacem, H. Alawadhi, M. Gaidi, Confined assembly of size-tunable silver nanoprisms on flexible Teflon tapes as highly active SERS hotspots for ultralow-level sensing of DNA and glucose, *Sensors and Actuators B: Chemical*. 398 (2024) 134780. https://doi.org/10.1016/j.snb.2023.134780.

[30] H.A. Ezzat, M.A. Hegazy, R. Ghoneim, H.Y. Zahran, I.S. Yahia, H. Elhaes, A. Refaat, M.A. Ibrahim, DFT and QSAR studies of PTFE/ZnO/SiO_2 nanocomposite, *Scientific Reports*. 13 (2023) 9696. https://doi.org/10.1038/s41598-022-19490-0.

[31] H. Izadi, B. Zhao, Y. Han, N. McManus, A. Penlidis, Teflon hierarchical nanopillars with dry and wet adhesive properties, *Journal of Polymer Science Part B: Polymer Physics*. 50 (2012) 846-851. https://doi.org/10.1002/polb.23076.

[32] I. Luzinov, D. Julthongpiput, A. Liebmann-Vinson, T. Cregger, M.D. Foster, V.V. Tsukruk, Epoxy-terminated self-assembled monolayers: molecular glues for polymer layers, *Langmuir*. 16 (2000) 504-516. https://doi.org/10.1021/la990719r.

[33] M.A. Hussein, W.A. El-Said, B.M. Abu-Zied, J.W. Choi, Nanosheet composed of gold nanoparticle/graphene/epoxy resin based on ultrasonic fabrication for flexible dopamine biosensor using surface-enhanced Raman spectroscopy, *Nano Convergence*. 7 (2020) 15. https://doi.org/10.1186/s40580-020-00225-8.

[34] Y. Zhang, C. Chen, R. Wang, G.I. Waterhouse, X. Qiao, Y. Sun, Z. Xu, Internal standard-based self-assembly Ag@4-MBN@Ag nanoarray SERS ratio sensor for sensitive detection of deltamethrin in foods, *Sensors and Actuators B: Chemical*. 412 (2024) 135786. https://doi.org/10.1016/j.snb.2024.135786.

[35] H. Wang, C. Wang, Q. Nie, R. Liu, Y. Yang, J. Lin, B. Zhang, R. You, Y. Liu, X. Xiao, Y. Lu, Polymer composite membranes as SERS substrate materials: recyclable and highly stable, *Chemical Engineering Journal*. 490 (2024) 151565. https://doi.org/10.1016/j.cej.2024.151565.

[36] Y. Song, K. Xiao, Q. Chen, X.D. Zhang, Z. Yu, W.W. Chen, X.B. Zhang, D. Zhang, D.J. Ni, P. Liang, Fabrication of GO/Fe3O4@Au MNPs for magnetically enriched and adsorptive SERS detection of bifenthrin, *Chemosensors*. 11 (2023) 73. https://doi.org/10.3390/chemosensors11020073.

[37] M.A. Hussein, W.A. El-Said, B.M. Abu-Zied, J.W. Choi, Nanosheet composed of gold nanoparticle/graphene/epoxy resin based on ultrasonic fabrication for flexible dopamine biosensor using surface-enhanced Raman spectroscopy, *Nano Convergence*. 7 (2020) 15. https://doi.org/10.1186/s40580-020-00225-8.

[38] T. Kameda, K. Ohkuma, S. Oka, Polytetrafluoroethylene (PTFE): a resin material for possible use in dental prostheses and devices, *Dental Materials Journal*. 38 (2019) 136-142. https://doi.org/10.4012/dmj.2018-088.

[39] J. Jiang, S. Zou, L. Ma, S. Wang, J. Liao, Z. Zhang, Surface-Enhanced Raman Scattering Detection of Pesticide Residues Using Transparent Adhesive Tapes and Coated Silver Nanorods, *ACS Appl. Nano Mater*. 1 (2018) 2431-2438. https://doi.org/10.1021/acsanm.8b00596.

[40] X. Li, L. Li, Y. Wang, X. Hao, C. Wang, Z. Yang, H. Li, Ag NPs@PDMS nanoripple array films as SERS substrates for rapid in situ detection of pesticide residues, *Opt. Mater*. 121 (2021) 111592. https://doi.org/10.1016/j.optmat.2021.111592.

[41] P. Sharma, N. Haq, M. Ahmad, K.A. Siddiqui, Mo@Zinc-CP composite for dual applications: luminescent detection of pesticides and photodegradation of organic dyes, *Journal of Molecular Structure*. 1327 (2025) 141249. https://doi.org/10.1016/j.molstruc.2024.141249.

[42] N. Liu, C. Xiao, W. Duan, N. Wang, B. Cui, Preparation of an imidazolium-based poly (ionic liquid) functionalized magnetic three-dimensional graphene oxide for magnetic solid phase extraction of pyrethroids from tea samples, *Journal of Chromatography B*. 1247 (2024) 124321. https://doi.org/10.1016/j.jchromb.2024.124321.

[43] Y. Wang, X. Cui, R. Lu, H. Gao, H. Li, W. Zhou, Dual-mode detection of fluorine-containing pesticides (bifenthrin, flufenoxuron, diflubenzuron) via ratiometric fluorescence and the Tyndall effect of fluorescent organic nanoparticles, *Food Chemistry*. 399 (2022) 134008. https://doi.org/10.1016/j.foodchem.2022.134008.

[44] S. Bhandari, B. Sen, S. Khatua, L.R. Singh, V.S. Parihar, M. Mahato, Ruthenium complex based nanocomposite film with enhanced and selective electrochemical sensing of bifenthrin pesticide, *RSC Advances*. 14 (2024) 29542-29558. https://doi.org/10.1039/d4ra04188g.

[45] A.A. Bletsou, A.H. Hanafi, M.E. Dasenaki, N.S. Thomaidis, Development of specific LC-ESI-MS/MS methods to determine bifenthrin, lufenuron, and iprodione residue levels in green beans, peas, and chili peppers under Egyptian field conditions, *Food Analytical Methods*. 6 (2013) 1099-1112. https://doi.org/10.1007/s12161-012-9515-2.